Tellus (2006), 58B, 463–475
Printed in Singapore. All rights reserved

TELLUS

A test of sensitivity to convective transport in a global atmospheric CO_2 simulation

By H. BIAN[1]*, S. R. KAWA[2], M. CHIN[2], S. PAWSON[2], Z. ZHU[2], P. RASCH[3] and S. WU[4],
[1]*UMBC Goddard Earth Science and Technology Center, NASA Goddard Space Flight Center, Greenbelt, MD 20771, USA;* [2]*NASA Goddard Space Flight Center, Greenbelt, MD 20771, USA;* [3]*National Center for Atmospheric Research, Boulder, CO 80307, USA;* [4]*Harvard University, Cambridge, MA 02138, USA*

(Manuscript received 9 January 2006; in final form 3 July 2006)

ABSTRACT

Two approximations to convective transport have been implemented in an offline chemistry transport model (CTM) to explore the impact on calculated atmospheric CO_2 distributions. Global CO_2 in the year 2000 is simulated using the CTM driven by assimilated meteorological fields from the NASA's Goddard Earth Observation System Data Assimilation System, Version 4 (GEOS-4). The model simulates atmospheric CO_2 by adopting the same CO_2 emission inventory and dynamical modules as described in Kawa et al. (convective transport scheme denoted as Conv1). Conv1 approximates the convective transport by using the bulk convective mass fluxes to redistribute trace gases. The alternate approximation, Conv2, partitions fluxes into updraft and downdraft, as well as into entrainment and detrainment, and has potential to yield a more realistic simulation of vertical redistribution through deep convection. Replacing Conv1 by Conv2 results in an overestimate of CO_2 over biospheric sink regions. The largest discrepancies result in a CO_2 difference of about 7.8 ppm in the July NH boreal forest, which is about 30% of the CO_2 seasonality for that area. These differences are compared to those produced by emission scenario variations constrained by the framework of Intergovernmental Panel on Climate Change (IPCC) to account for possible land use change and residual terrestrial CO_2 sink. It is shown that the overestimated CO_2 driven by Conv2 can be offset by introducing these supplemental emissions.

1. Introduction

The importance of characterizing transport error in forward models has been widely recognized, and substantial effort has been devoted to quantifying such error (e.g. Denning et al., 1999; Engelen et al., 2002; Palmer et al., 2003). Tropospheric constituent transport occurs by advective, diffusive and convective processes and inadequacies in any of these mechanisms will lead to error in simulated trace gas concentrations. The primary goal of this study is to explore the extent to which the treatment of convective transport impacts the atmospheric CO_2 distribution. The study uses a chemistry transport model (CTM) with specified surface flux distributions and perturbs the representation of convective transport in this system, while all other processes are held fixed. The two approximations to convective transport are referred to as Conv1 and Conv2. Following Kawa et al. (2004), Conv1 uses a constraint of the total convective mass flux (CMF), in which air parcels entrained at cloud base are transported upwards, detraining at a rate proportional to the convergence of CMF. Conv2 is a potentially more accurate approximation, using information on updraft and downdraft, as well as entrainment and detrainment rates; this allows for air parcels to be ventilated within the entire cloud ensemble and also to enter or leave the cloud environment at any altitude, subject to the same constraints on total CMF. All fields used were archived as 3 h averages from the Goddard Earth Observation System Version 4 (GEOS-4) data assimilation system (Bloom et al., 2005). Hence, the two algorithms represent cloud convective transport from a very simple to a relatively complex form. The uncertainty induced by them will represent one term in the potential cloud convection error. We will further identify regions where mixing ratios are sensitive to atmospheric convection, with an overall goal to assist regional carbon cycle simulation. This study complements a number of other approaches to quantifying transport uncertainty, in at least two ways.

First, several studies have attempted to quantify the differences between atmospheric transport using different algorithms of atmospheric convection. Mahowald et al. (1995) used a column model to quantify transport differences among seven different cumulus convection parameterizations, illustrating vastly different results that are sensitive to aspects of 'closure' (the criteria used to determine onset of convection, dependent on some

*Corresponding author.
e-mail: Bian@code916.gsfc.nasa.gov
DOI: 10.1111/j.1600-0889.2006.00212.x

aspect of horizontal mass convergence below cloud base) and to the cloud assumptions used in the convection module itself. Gilliland and Hartley (1998) demonstrated, using two versions of a GCM in which the CMF differs substantially, that the strength of convective transport has a discernable impact on interhemispheric exchange of long-lived trace gases. Olivie et al. (2004) also found significantly different radon distributions in the upper troposphere and lower stratosphere in their simulations with convective mass fluxes from two different resources [one archived from the European Center for Medium-Range Weather Forecasts (ECMWF) and another from off-line diagnoses calculated with a parameterization that mimics the ECMWF-scheme using archived winds, pressures, temperatures, specific humidities and evaporation rates]. The present study differs from these previous works in that here the GEOS-4 convection scheme to produce the cloud field is not changed, but the manner in which the archived CMF fields are used in the CTM does change.

Second, a number of studies have examined transport of trace gases using different meteorological fields and/or different CTMs. At the forefront of such comparison is the Atmospheric Tracer Transport Model Intercomparison Project (TransCom), which was created to quantify and diagnose the uncertainty in inverse calculations of the global carbon budget that resulted from errors in simulated atmospheric transport (Law et al., 1996, Denning et al., 1999, Gurney et al., 2003). These multimodel assessments indicate that the model behaviour differs substantially; however, it is difficult to diagnose the determining factors that cause these difference since the participating models are different not only in convective parameterization but also in spatial resolution, advection schemes and most importantly, meteorological fields (Gurney et al., 2003). Our approach presented here allows testing of the convection uncertainty within a single model framework and driven by the same meteorological fields, therefore eliminating all compounding perturbing factors other than the model convective transport methodology. The information of where, when, and how large are CO_2 uncertainties induced by different convection schemes will also be useful to interpret inverse studies using our CTM. Note that this approach does not address the most fundamental issues related to the ability of the parent general circulation model to correctly capture the location and strength of convection events but focuses on the application of CMF for long-lived trace gas transport.

An additional goal of this study is to examine the sensitivity of atmospheric CO_2 to its regional source/sink uncertainty. The study of model convection transport raises a question: which cloud convective scheme is more appropriate to manifest atmospheric vertical transport in the context of model-measurement agreement? The answer is not simple, since the simulation capability also depends on constraint of the CO_2 source/sink. Global decadal budgets summarized for the 1980s and 1990s infer a large residual terrestrial sink for atmospheric CO_2 with attached uncertainty of 50–100% or more (IPCC, 2001). This so-called 'missing sink' for CO_2 epitomizes a major uncertainty in the current understanding of carbon cycle processes. In this study, in addition to a 'standard' emission scenario (Emi1) proposed by TransCom3, we construct two residual terrestrial CO_2 fluxes (with the total emissions referred as Emi2 and Emi3) that are constrained within the IPCC, 2001 CO_2 to address the following questions: (1) How sensitive is atmospheric CO_2 change in response to its regional source/sink change? (2) Is the variation of atmospheric CO_2 inferred from surface flux uncertainty comparable to the variation induced from changing convective transport representations?

This paper starts with a description of the model framework in Section 2, in particular the two convection approximations. The observational data and the potential errors in model-observational comparisons due to different spatial and temporal resolutions in data are also explained in Section 2. Section 3 presents the CO_2 simulation uncertainties in a single forward model framework that are induced by two different convection approaches and by three emission scenarios. Conclusions and implications of this work are given in Section 4.

2. Description of model and data

2.1. Model framework

An offline CTM framework has been designed in such a way that each physical and chemistry module can be upgraded easily through an interface. The goal of developing such an offline CTM is to assess the impacts on tracer distributions due to the different dynamical and chemical approaches. For this study, the advection algorithm adopts the code of Lin and Rood (1996), which is formulated in flux form and employs a semi-Lagrangian algorithm. This advection algorithm has been extensively evaluated in tropospheric and stratospheric CTMs (Lin and Rood, 1996; Bey et al., 2001; Chin et al., 2002; Douglass et al., 2003) and implemented in several global chemistry and transport models including a trace gas transport model (PCTM) (Kawa et al., 2004) and the Goddard Chemistry Aerosol Radiation and Transport (GOCART) model (Chin et al. 2002, 2004). Boundary layer turbulence and atmospheric diffusion is calculated from the diffusion equation, same as in GOCART and PCTM. Since our study focuses on the representation of convective transport in a CTM, we will describe in detail the two cloud convection approximations in Section 2.2. The model, in this study, is driven by time-averaged analysed meteorological fields from NASA's GEOS-4 assimilation system (Bloom et al., 2005).

A 'standard' emission scenario (denoted as Emi1) based on the compilations of TransCom 3 (Gurney et al., 2002) is used in our convection transport uncertainty study. Emi1 comprises a fossil fuel combustion with a global total of 6.17 Pg C yr^{-1} in 1995 (Andres et al., 1996), a seasonally balanced terrestrial biosphere based on computations of net primary productivity from the Carnegie–Ames–Stanford Approach (CASA) (Randerson et al., 1997), and an air–sea gas exchange (-2.2 Pg C yr^{-1}) from

$1^\circ \times 1^\circ$ monthly mean CO_2 fluxes derived from sea-surface pCO_2 measurements (Takahashi et al., 2002). CO_2 source oxidized from the reduced carbon trace gases (CO, CH_4, and NMVOCs) is accounted simply as part of the fossil fuel emission at the surface. While the fossil fuel emission is given as annual mean rates, the fluxes from biosphere and ocean are provided as monthly means which are compiled from the diurnal averages. All sources/sinks are dealt in the surface layer of the model. The potential errors in reproducing atmospheric CO_2 due to using monthly mean fluxes had been discussed in Kawa et al. (2004); the diurnal cycle of biospheric CO_2 is weakened in the planetary boundary layer (PBL) in source/sink regions. Suntharalingam et al. (2005) reported the potential errors of simulated CO_2 due to releasing reduced carbon at surface. We will address this in Section 3.1.1 when comparing simulated surface CO_2 with observations.

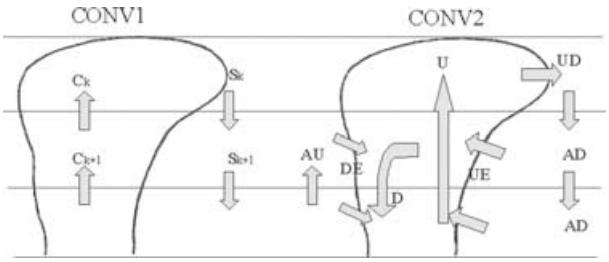

Fig. 1. Schematics of the cloud mass fluxes for Conv1 (C: total cloud mass flux; S: compensating large-scale subsidence) and Conv2 (U: updraft; UE: updraft entrainment; UD: updraft detrainment; AD: environment subsidence to compensate in-cloud updraft; D: downdraft; DE: downdraft entrainment; AU: environment upward to compensate in-cloud downdraft). The shallow cloud model for Conv2 (not shown in figure) is similar to Conv1.

2.2. *Representation of convective transport*

A suite of meteorological and physical fields is archived from GEOS-4. For transport studies, Bloom et al. (2005) describe the utility of time-averaged meteorological data (winds and temperatures) along with tendencies from the physical parameterizations in the underlying GCM. Convection in GEOS-4 is represented by two models: deep convection follows Zhang and McFarlane (1995) while shallow convection is based on Hack et al. (1994). The parameterization of deep convection in GEOS-4 introduced the concepts of updraft and downdraft, as well as the entrainment and detrainment associated with the updraft and downdraft, to describe penetrative cumulus convection (Zhang and McFarlane, 1995). Moist upward convection is initiated when there is convective available potential energy (CAPE) for reversible ascent of an undiluted parcel from the subcloud layer. Each updraft is represented as an entraining plume with a characteristic fractional entrainment rate. Detrainment associated with updraft is confined to a thin layer near the plume top where the mass carried upward is expelled into the environment. Downdrafts are assumed to exist when there is precipitation production in the updraft ensemble. The downdrafts start at or below the bottom of the updraft detrainment layer and penetrates down to the subcloud layer. A complete set of CMF data is archived from the shallow and deep convection modules, as described below.

Table 1 shows the main features and differences of the two convective transport approaches tested in this study. These are represented schematically in Fig. 1. The first cloud convection scheme (Conv1) was implemented in PCTM and used to simulate atmospheric CO_2 distribution (Kawa et al., 2004). This is a semi-implicit convective module, constrained by the subgrid-scale cloud mass flux from the assimilation system. Vertical cloud transport in layer k is calculated by

$$q_k^{t+\Delta t} - q_k^t = \frac{g\,\Delta t}{\Delta p_k}[C_{k+1}(q_{k+1} - q_k) - C_k(q_k - q_{k-1})]^{t+\Delta t/2}, \qquad (1)$$

where q is the tracer concentration, and C_k, C_{k+1} are the net convective mass fluxes (shallow and deep convection updraft minus downdraft) at the upper and lower edges of a layer, t is the model time step, and $\Delta p_k/g$ is the air mass of a layer. The term on the right-hand side of the equation calculates the tracer mass change in layer k due to cloud fluxes and this tracer mass change is taken at the middle of the time step (semi-implicit).

The second convective transport algorithm (Conv2) uses additional output from the shallow (Hack et al., 1994) and deep (Zhang and McFarlane, 1995) convection codes and is designed to be consistent with the subgrid cloud parameterizations

Table 1. The summarization of main features and differences in two convection schemes

	Conv1	Conv2
References	Kawa et al. (2004)	Collins et al. (2004)
Implemented in	PCTM	MATCH; GEOS-CHEM
Differentiate tracer in & out cloud	No	Yes
Numerical scheme	Semi-implicit	Upstream differencing
Differentiate shallow and deep cloud in CTM	No	Yes
Constrained by	Cloud mass flux	Shallow: shallow cloud mass flux; overshoot parameter Deep: updraft; downdraft; updraft entrainment; updraft detrainment; downdraft entrainment

developed in GCM. It has been implemented in several global models (Eneroth et al., 2003a; Zender et al., 2003; Li et al., 2005; Millet et al., 2005). Shallow convection uses cloud mass fluxes and overshoot parameters from the Hack scheme to mix the passive constituents in layers $k-1$ through $k+1$ for the vertical k layer. This transport is essentially the same as that done in Conv1. The deep convection distinguishes the mass fluxes among updraft, downdraft, updraft entrainment, updraft detrainment and downdraft entrainment, and employs all of them to drive cloud vertical mixing. It uses simple first order upstream biased finite differences to solve the steady-state mass continuity equations for the 'bulk' updraft and downdraft mixing ratios and the mass continuity equation for the gridbox mean (Collins et al., 2004).

$$\frac{\partial(M_{\mathrm{x}}q_{\mathrm{x}})}{\partial p} = E_{\mathrm{x}}q_{\mathrm{e}} - D_{\mathrm{x}}q_{\mathrm{x}} \tag{2}$$

$$\frac{\partial \bar{q}}{\partial t} = \frac{\partial}{\partial p}[M_{\mathrm{u}}(q_{\mathrm{u}} - \bar{q}) + M_{\mathrm{d}}(q_{\mathrm{d}} - \bar{q})] \tag{3}$$

The subscript x is used to denote the updraft (u) or downdraft (d) quantity. Here, M_{x} is the mass flux in units of Pa s^{-1} defined at the layer interfaces, q_{x} is the mixing ratio of the updraft or downdraft. q_{e} is the mixing ratio of the quantity in the environment (that part of the grid volume not occupied by the up and downdrafts), and is assumed to be the same as the gridbox averaged mixing ratio $\overline{q}$. E_{x} and D_{x} are the entrainment and detrainment rates (units of s^{-1}) for the up- and downdrafts. Updrafts are allowed to entrain or detrain in any layer. Downdrafts are assumed to only entrain and all of the mass is assumed to be deposited into the surface layer. The tracer mass flux and mixing ratio are integrated along the pressure p and time t, respectively.

Conv2 in our CTM takes full advantage of the underlying GCM cloud parameterization to transport tracers. The algorithm of Conv2 solves three variables: tracer-mixing ratios in cloud updraft, cloud downdraft, and environment by considering tracer mass changes associated with these regimes (eqs. 2–3). The objective of Conv2 is to keep the tracer vertical transport in a penetrating cumulus as efficient as the energy and moisture transport in its underlying GCM. For example, in a cloud updraft regime, Conv2 sucks in environmental tracer into cloud through the updraft entrainment flux at the low part of the cloud and then transports the tracer upward inside the updraft regime with the updraft flux. When the cloud reaches a level where updraft detrainment appears, usually at the top part of a deep cloud, Conv2 begins to return the tracer to the environment in the proportion to the cloud updraft detrainment. In this way, Conv2 can efficiently transport tracer vertically inside cloud updraft (and downdraft) and affect environment tracer mixing ratio through cloud convergent (entrainment) and divergent (detrainment) fluxes.

On the other hand, Conv1 uses only the total net cloud flux to solve a layer's mean mixing ratio by exchanging with adjacent layers. There are two limitations in this approach: (1) tracer transport cannot proceed unmixed through more than one vertical gridcell per time step in a penetrative cumulus; (2) the fluxes in opposite directions (updraft versus downdraft) are cancelled out by an equivalent amount in the total cloud mass flux. This will decrease convective mixing relative to treating up and down drafts separately, although the downdraft component is generally small (see below). Note that the reality of transport by either method depends on the reality of subgrid-scale physical parameterization in the parent GCM, which is highly uncertain and representative only in a statistical sense in current models (Mahowald et al., 1995).

2.3. Observational data

The observational data of atmospheric CO_2 mixing ratio used to evaluate model simulation are obtained from NOAA Climate Monitoring and Diagnostics Laboratory (CMDL) Carbon Cycle Greenhouse Gases (CCGG) (http://www.cmdl.noaa.gov/ccgg/index.html). Samples are taken at NOAA CMDL Carbon Cycle Cooperative Global Air Sampling Network sites. They are measured by a non-dispersive infrared absorption technique in air samples collected in glass flasks. Samples are collected in pairs approximately once a week at local noon for 41 surface (non-baseline) fixed sites and aircraft measurement over 14 sites are made usually one to two times per month in local afternoon. The pair difference is calculated, and samples with a pair difference greater than 0.5 ppm are flagged. Flagged data are excluded from our comparisons.

There are spatial and temporal resolution differences between observational and simulated data. The model results are daily or monthly averages at 2 latitude $\times$ 2.5 longitude spatial resolution, while observational data are 'instantaneous' taken several times per month at specific site locations. Spatial mismatch of simulation (grid mean value) and measurement (site location) leads to 'representation error' and temporal covariance between mixed-layer height and biosphere-atmosphere exchange fluxes may cause biases, 'rectification errors', over diurnal or seasonal timescales (Denning et al., 1996; Gerbig et al., 2003; Yi et al., 2004). Furthermore, the 'representation error' is not fixed because footprint (the surface area inside which the data are correctly represented by the measurement at a site) varies with height, wind direction, meteorological conditions (stability) and the magnitude of the CO_2 flux (Rannik et al., 2000; Aubinet et al., 2001; Eneroth et al., 2003, Murayama et al., 2004). An investigation of the footprint in a measuring site in western Siberia indicated that it is only ten to 100 km in July but much larger in winter (Eneroth et al., 2003b). The CO_2 Budget and Rectification Airborne (COBRA) study in August 2000 also pointed out that models require horizontal resolution finer than $\sim$30 km to fully resolve spatial variations of atmospheric CO_2 in the boundary layer over the continent (Gerbig et al., 2003). Therefore, the inherent features in the simulation and model data will result in the differences in model-observation comparisons even for an ideal simulation, and the errors vary with time and location.

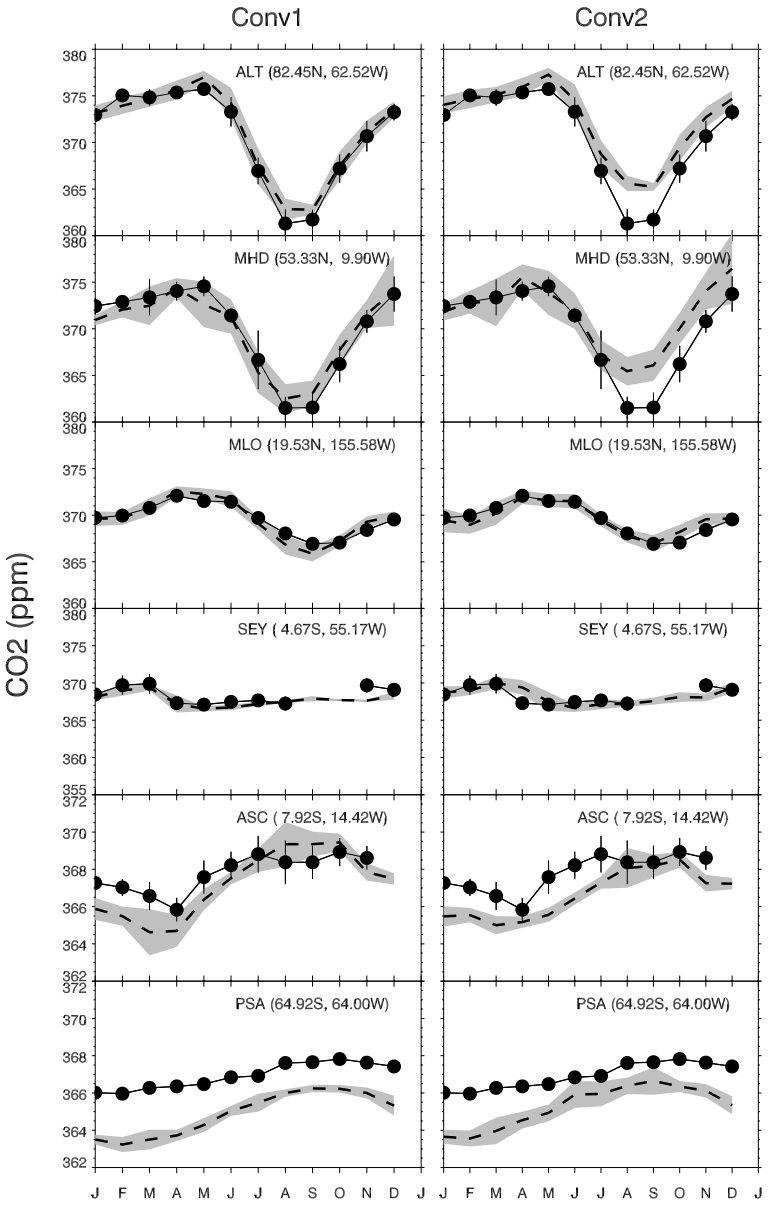

Fig. 2. Surface CO_2 (ppm) comparisons between standard simulation (using Emi1 and Conv1) and CMDL measurement (left-hand column). Monthly mean CO_2 and its standard deviation are represented by dot-line and bar for CMDL and by dash-line and shade area for model simulation, respectively. Model mixing ratio has been adjusted by a constant offset value so that the annual mean at Mauna Loa equals that of the observation (Kawa et al., 2004). Also shown in figure is surface CO_2 simulated with the same conditions as left-hand column but with convection scheme Conv2 (right-hand column).

3. Results and discussions

3.1. The impacts of cloud convection schemes on atmospheric CO_2 distributions

3.1.1 Surface concentrations. The CO_2 surface concentrations from our standard simulation with Conv1 and Emi1 (basically the same setup as in Kawa et al., 2004) are compared with the CMDL observations in Fig. 2 (left-hand column). The model captures surface CO_2 magnitude and seasonal variation, but underestimates CO_2 at Southern Hemisphere (SH) high latitudes in comparison with CMDL measurements. The sudden shift of CO_2 mixing ratio is evident in influence from the Northern Hemisphere (NH) to SH in Mahe Island, Seychelles (SEY: 55.2N, 4.7S) during March to April as the Inter-Tropical Convergence Zone (ITCZ) moves north and the atmospheric CO_2 concentration drops to levels typical of the SH. These performances are the same as those shown in Kawa et al. (2004). The low CO_2 in the SH high latitudes is perhaps partially induced by accounting reduced carbon as part of fossil fuel emission and releasing it at surface in our current simulation. In the real atmosphere, CO_2 is produced from reduced carbon trace gases in the atmosphere. A CO_2 source of 0.9–1.3 Pg C yr^{-1} from reduced trace gases (Suntharalingam et al., 2005) is comparable in magnitude to estimates of annual mean ocean biosphere CO_2 sinks (IPCC, 2001). A recent study points out that including the reduced carbon oxidation in the atmosphere, not at the surface, will result in an enhancement of southern hemispheric CO_2 (Suntharalingam et al., 2005).

In order to investigate the impacts of different convective transport algorithms on atmospheric CO_2 distributions, we run the model with the Conv2 convective transport scheme described in Section 2.2. Figure 2 shows the comparisons of model simulations from Conv1 and Conv2 with observations at selected CMDL surface sites for their representativeness of major geographic locations and distinct features of carbon emission fluxes: NH high latitude (ALT), NH mid-latitude land regions (MHD), NH background (MLO), tropical regions (SEY), SH biomass burning (ASC), and SH high latitude (PSA).

While Conv1 captures the observed seasonal variation of CO_2 at station ALT, Conv2 shows a significant summer enhancement, thus a reduced magnitude of such variation. For example, the minimum CO_2 mixing ratio in the summer is 362.2 ppm in Conv1 but 366.0 in Conv2 at ALT; consequently, the CO_2 seasonal amplitude is 14.5 ppm in Conv1 but only 11.0 ppm in Conv2. A sharp decrease of CO_2 mixing ratio from March to April observed at station SEY is captured by Conv1, whereas not by Conv2. This means that Conv2 does not represent the tracer variation during the ITCZ transition. Both convective approximations underestimate CO_2 during the first half of the year at station ASC, however, the CO_2 seasonality of Conv1 is closer to that of observations.

To further reveal where and when the biggest discrepancies occur between the two convection transport approaches, we plot in Fig. 3 the global surface CO_2 mixing ratios in January and July simulated with Conv1 and Conv2. The differences of the surface CO_2 mixing ratios between Conv1 and Conv2 in January are small. The maximum values are 373.30 and 375.32 ppm while the minimum values are 343.95 and 346.30 ppm for Conv1 and Conv2, respectively. The simulations point out that Conv2 enhances the global CO_2 mixing ratio at the surface by about 2 ppm globally, and horizontal distributions (gradient between high and low CO_2) remain virtually unchanged. On the other hand, the surface CO_2 concentrations in July differ substantially between Conv1 and Conv2, particularly in the NH boreal forest region where Conv2 demonstrates a substantial CO_2 enhancement. While the maximum values are similar between Conv1 and Conv2 (363.82 ppm in Conv1 and 363.09 ppm in Conv2), the minimum values are significantly different (335.30 ppm in Conv1 and 343.11 ppm in Conv2). The difference in the July minimum values over southern Siberia is 7.8 ppm, which is nearly 30% of the magnitude of seasonal variation of 25 ppm simulated with Conv1.

Surface CO_2 exhibits larger NH values in Conv2 than in Conv1 in July. This may indicate that Conv2 has stronger vertical transport in July when the NH biosphere serves as a CO_2 sink. We will explore the reason for this performance in the following subsections. We also tested a third convective transport implementation, which has been used in simulations with the previous version of the GEOS meteorological output (GEOS-3) (Chin et al., 2002, 2004; Suntharalingam et al., 2005), and found results from

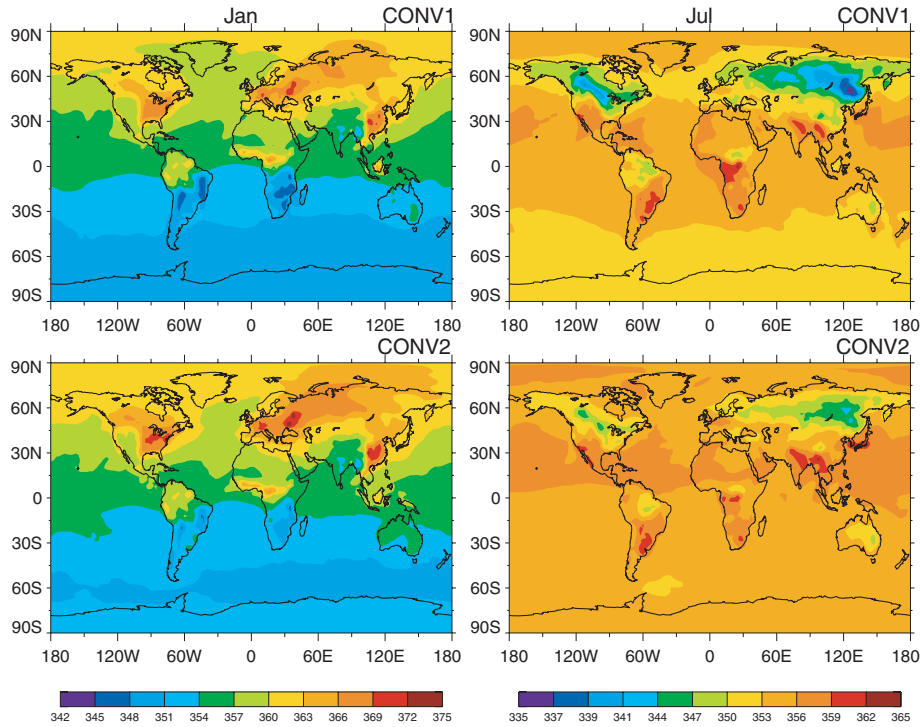

Fig. 3. CO_2 (ppm) surface contours in January (left-hand panel) and July (right-hand panel) using two convective schemes with Emi1. Note that significant CO_2 difference due to two convective schemes occurs over boreal forest regions in July.

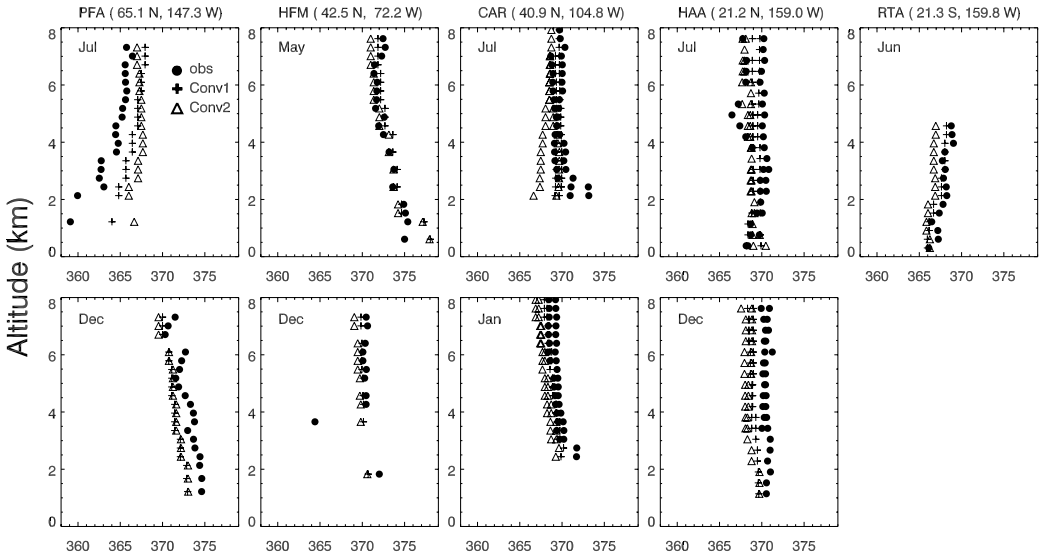

Fig. 4. The comparisons of observed CO_2 vertical values (dot) with simulated CO_2 using Conv1 (plus) and Conv2 (triangle) at five CMDL airplane observation sites. The model data is daily average on the observational day. There are one to two observations during each month at each station. Stations PFA, HFM, CAR and HAA have comparisons at one summer month and one winter month, but station RTA gives comparison at only one summer month.

that method intermediate to those from Conv1 and Conv2 shown here.

3.1.2 Vertical distributions. Convective transport generally reduces the vertical gradient of constituents with surface sources or sinks. Aircraft profiles are made available from the CMDL long-term regular measurements. Five out of 14 sites provide measurements for comparison in the year 2000. These five sites represent different carbon environments: NH boreal forest (Poker Flats Alaska, PFA), continental pollutant (Harvard Forest Massachusetts, HFM), continental background (Carr Colorado, CAR), NH remote ocean (Molokai Hawaii, HAA) and SH remote ocean (Raratonga Cook Islands, RTA). The vertical profiles of simulation and measurement of CO_2 mixing ratios at the five sites are shown in Fig. 4 for the two different transport schemes. We demonstrate the comparisons for one summer month and one winter month subject to the availability of observations. Generally the simulation agrees well with the measurements. The large discrepancies between model and observation occur mostly inside the PBL in the summer over continental stations. For example, observed CO_2 over station PFA shows strong surface ecosystem uptake in July which is not fully captured in the simulations with either convection approach. This implies that summer boreal forest CO_2 uptake around station PFA may be not strong enough in the model's surface flux compilation. Higher CO_2 in the PBL over continental station CAR during both summer and winter indicates that a possible local source may not be well captured in the model. Using the Emi1 emission scenario, the simulated CO_2 using Conv1 matches observations better than that of Conv2, which is consistent with the diagnosis for surface CO_2 mixing ratio. Furthermore, CO_2 simulated by Conv1 and Conv2 often differs more in the middle troposphere than PBL except stations PFA and CAR in summer, indicating that the CO_2 perturbation due to using two convection schemes may be globally discernable in the middle troposphere.

A series of sensitivity experiments are designed to demonstrate how representations of the archived GCM shallow and deep convection fluxes in the offline CTM transport control atmospheric CO_2 three-dimensional distributions. CO_2 is simulated for 5 days in early January and July under two pairs of circumstances: without advection and diffusion but with Conv1 (Conv1-only) or Conv2 (Conv2-only); with advection and diffusion and plus Conv1 (Conv1-adv-diff) or Conv2 (Conv2-adv-diff). All experiments adopt Emi1 and start with a flat initial CO_2 field of 350 ppm.

The vertical profiles of the 5-d mean CO_2 change at a NH boreal forest site (Site A: 50.0N, 122.5E), as well as the corresponding mean cloud fluxes, are plotted in Fig. 5. Site A is dominated by shallow cloud convection in January; the simulation indicates that the vertical profiles of the CO_2 change due to Conv1-only and Conv2-only are close to each other with a slightly higher vertical transport in Conv1. The involvement of advection and diffusion dilutes high CO_2 near the surface source to wider regions, so that the changes of CO_2 are smaller in the near-surface but the changes extend to higher levels in the cases of Conv1-adv-diff and Conv2-adv-diff.

Site A in July, on the other hand, experiences both shallow and deep cloud convection. The vertical profiles of the change of CO_2 differ dramatically for the two convective approximations. The profile using Conv1 varies smoothly in the vertical, while the profile using Conv2 shows maximum and minimum CO_2 change at different vertical ranges. It is relative easy to understand the smooth vertical CO_2 change from Conv1 because

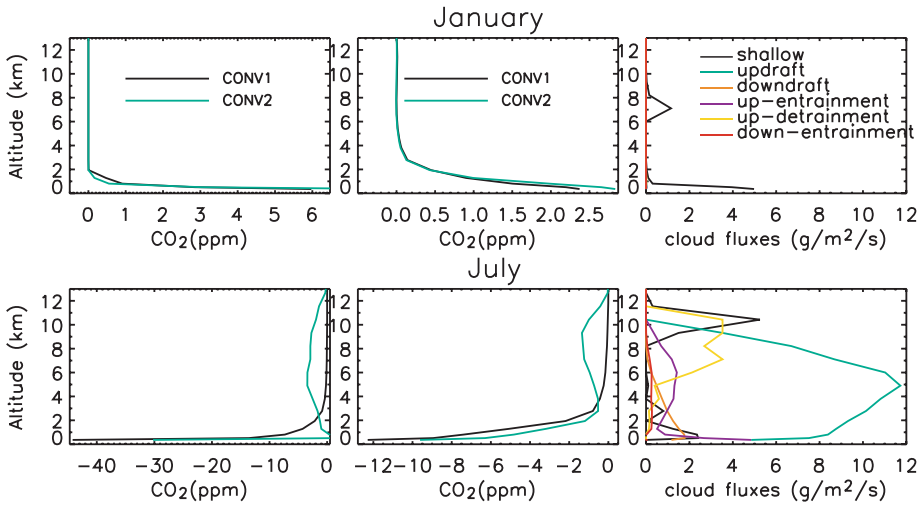

Fig. 5. Comparisons of 5-d mean CO_2 change vertical profiles between Conv1 (black) and Conv2 (green) at a NH boreal forest site (50.0N, 122.5E) in January (upper panel) and July (lower panel) for two kinds of sensitivity runs: without advection and diffusion (left-hand column) and with advection and diffusion (middle column). All simulations use Emi1 and start with a flat CO_2 initial field of 350 ppm. Also shown in the figure are the corresponding 5-d mean cloud mass fluxes (right-hand column) associated with shallow cloud (black) and each deep cloud component: updraft (U, green), downdraft (D, orange), updraft entrainment (UE, blue), updraft-detrainment (UD, yellow), and downdraft entrainment (DE, red).

this approximation mixes a layer mean CO_2 mixing ratio with its adjacent layers under the constraint of the total cloud flux. However, Conv2 uses the updraft and downdraft movements produced by the GCM separately to transport CO_2 in deep cloud convection. The cloud fluxes from each deep cloud component (Fig. 5 (lower right hand panel)) show that the deep cloud convection in Site A during this time period occurs in the entire troposphere with updraft flux (U) extending from near surface to over 10 km, updraft detrainment (UD) starting around 5 km with a peak value around 10–11 km, and downdraft flux (D) starting at the bottom of the updraft detrainment region and increasing downward to the bottom of cloud. July NH boreal forest in Site A will produce a very low surface CO_2 mixing ratio due to a strong biospheric uptake during the forest growing season. As a consequence, updraft flux in Conv2 lifts the air in the lower part of cloud with low CO_2 mixing ratio and releases this air back to the environment at the upper part of the cloud controlled by the updraft detrainment flux. Through this deep cloud updraft movement and its interaction with the environment via entrainment and detrainment, Conv2 reduces the atmospheric CO_2 mixing ratio efficiently in the middle to upper troposphere. In addition to the strong updraft flux overshoot the low CO_2 from near surface directly to middle-upper troposphere, the downdraft flux used in Conv2 transports CO_2 from the middle troposphere downward. These processes limit the change of CO_2 mixing ratio near the bottom of cloud. However, near unchanged CO_2 mixing ratio at the bottom of cloud in Conv2-only seems still unrealistic. Similar to January, the involvement of advection and diffusion in July reduces the CO_2 gradient in the near surface and propagates the CO_2 change due to surface sink into wider areas.

The monthly mean CO_2 vertical profiles in January and July simulated with Conv1 and Conv2 for the year 2000 and the monthly mean cloud fluxes at site A are plotted in Fig. 6 to illustrate the long-term overall impacts on atmospheric CO_2 distributions due to using different convection approximations. For the continuous simulation, the monthly mean CO_2 mixing ratios in Fig. 6 also contain information on their initial distribution at the beginning of the corresponding month. Comparing with the vertical profiles obtained from the 5 day run (Fig. 5), the relationship of the monthly mean CO_2 profiles between Conv1 and Conv2 in Fig. 6 agrees generally, although the magnitude of CO_2 changes and the spatial ranges affected by the changes in the continuous simulations are different with that in the 5 day runs. Therefore, we can conclude that the significant enhancement of July surface CO_2 in the NH boreal forest Site A in Conv2 in the continuous run results from the stronger vertical tracer mass exchange in Conv2 due to the different approximations for the deep cloud convection adopted in the Conv1 and Conv2.

3.2. CO_2 simulations with different emission scenarios

The model simulations shown in Section 3.1 have revealed that Conv2 overestimates the CO_2 surface concentrations in summer season by 0–4 ppm while Conv1 agrees with observations better (Fig. 2) when the standard CO_2 flux (Emi1) was used. In this section, we use modified CO_2 flux scenarios (Emi2 and Emi3) to elucidate the sensitivities of CO_2 seasonal cycle to the source/sink variations.

Figure 7 shows the carbon budget terms and their uncertainties from each reservoir summarized in the recent report by the Intergovernmental Panel on Climate Change (IPCC, 2001). It

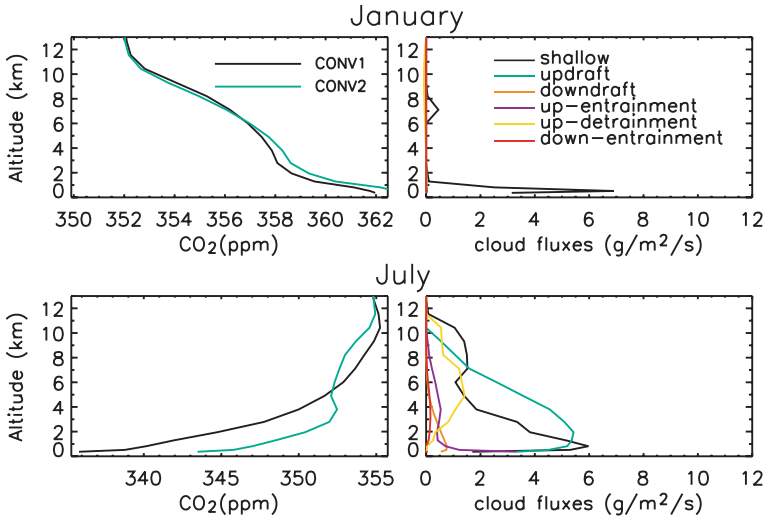

Fig. 6. Comparisons of monthly mean CO_2 vertical profiles (left-hand column) between Conv1 (black) and Conv2 (green) at a NH boreal forest site (50.0N, 122.5E) in January (upper panel) and July (lower panel). Also shown in the figure are the corresponding monthly mean cloud mass fluxes (right-hand column) associated with shallow and deep cloud.

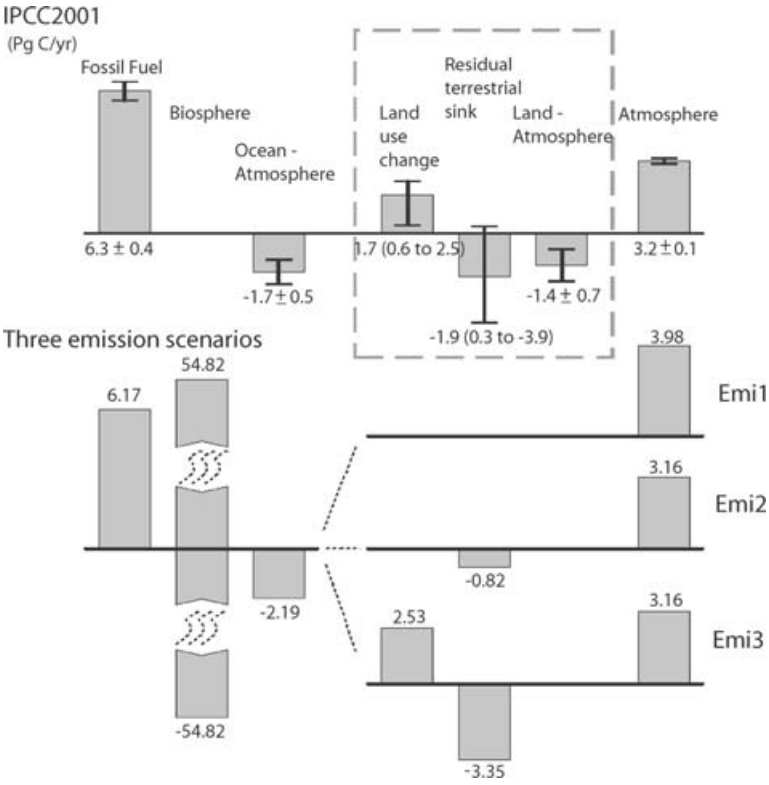

Fig. 7. The carbon budgets and uncertainties from each reservoir from IPCC, 2001 (upper panel) and three carbon emission scenarios adopted in the study (lower panel). All budgets from IPCC, 2001 are for the 1990s except the budgets inside the box which are for the 1980s. Standard emission scenario (Emi1) gives atmospheric carbon growth rate of 3.98 Pg C yr^{-1} which exceeds its range reported by IPCC, 2001. Residual terrestrial sink is imposed to eliminate the extra atmospheric carbon growth in Emi1 by applying global scaling factors of 0.06 for Emi2 to NEP when NPP exceeds RESP. Biomass burning emission from TRMM-based inventory in the year 2000 is adopted to account for land use change in Emi3 which is based on Emi2. This additional biomass burning source in Emi3 is balanced by further increase of biosphere uptake by a global factor of 0.185 from Emi1 to maintain the atmospheric CO_2 growth rate at 3.16 Pg C yr^{-1}. Unlike the other emissions which are given at surface level, biomass burning emission is distributed within the whole mixing layer.

also gives three emission scenarios adopted in this study. The budgets presented by IPCC, 2001 represent the summarized results from measurements and models for 1990–1999 except land use change and residual terrestrial sink which are for the 1980s. The processes inside the box are not well understood and are primarily responsible for the CO_2 'missing sink'. In the 'standard' emission scenario (Emi1), an annual balanced biosphere emission flux is compiled from net primary production (NPP) and heterotrophic respiration (RESP) to account for net ecosystem production (NEP). The ocean uptake (-2.19 Pg C yr^{-1}) (Takahashi et al., 2002) is not sufficient enough to compensate the fossil fuel source (6.17 Pg C yr^{-1}) (Andres et al., 1996), because the balance (3.98 Pg C yr^{-1}) exceeds the current atmospheric CO_2 growth rate (3.2 Pg C yr^{-1}) (IPCC, 2001). A 'missing' carbon sink is necessary to reconcile our atmospheric CO_2 observational facts (Tans et al., 1990; Gurney et al., 2002; Olsen and Randerson, 2004). Several lines of evidence suggest that the northern hemisphere terrestrial biosphere is responsible (Tans et al., 1990; Fan et al., 1998; Battle et al., 2000; Bousquet et al., 2000; Gerbig et al., 2003; Gurney et al., 2003, 2004; Maksyutov

et al., 2003). For example, compared to a seasonally balanced biosphere flux generated by the CASA model, CO_2 source fluxes inferred from the inversion require significant changes to the carbon exchange in the European region with greater growing season net uptake persisting into the fall months (Gurney et al., 2004). Boreal Asia also exhibits greater peak growing season net uptake (Gurney et al., 2004). The zonal mean surface concentration for the biospheric CO_2 shows more spread in the northern mid- to high-latitudes than for fossil fuel emissions (Gurney et al., 2003). Additional Siberian airborne observations lead to the projection of extra sinks in Boreal Asia of 0.2 Pg C yr^{-1}, and a smaller change for Europe (Maksyutov et al., 2003). Therefore, as a surrogate to our 'background' emission flux, we use two supplemental emission scenarios to account for the residual terrestrial sink and land use change that are consistent with the IPCC, 2001 budgets. Emi2, based on Emi1, enhances the seasonal uptake of NEP by a factor of 0.06 and maintains the efflux of NEP unchanged, that is, wherever and whenever the net flux is negative, uptake is scaled by 1.06. The additional biosphere uptake of 0.82 Pg C yr^{-1} would bring the atmospheric CO_2 growth rate from 3.98 Pg C yr^{-1} in Emi1down to 3.16 Pg C yr^{-1}, a better fit to the atmospheric observations.

Emi3, based on Emi2, gives an additional source from biomass burning to represent land use change. CO_2 from biomass burning emission in the year 2000 is obtained from TRMM-based inventory which was constructed using the approaches described in Van der Werf et al. (2003, 2004) and Randerson et al. (2005). The dataset is integrated using TRMM-VIRS hot spot data and burned area, updated with MODIS burned area for Africa, South America and Australia, and extended spatially and temporally using ATSR and AVHRR data. The total biomass burning emission of CO_2 is 2.53 Pg C yr^{-1} for the year 2000. This additional source is balanced by further increase of biosphere uptake by a factor of 0.185 from Emi1 to maintain the atmospheric CO_2 growth rate at 3.16 Pg C yr^{-1}. This approach is based on a multiple year timescale for plant grow-back. A large uncertainty in this approach is expected and the scenario is intended to represent an upper limit to the effect of biomass burning/land use change. As pointed out by IPCC, 2001, land use change is the category to have the lowest confidence in based on our knowledge of CO_2 surface fluxes. Unlike the other emissions which are given at surface level, biomass burning emission is distributed within the whole mixing layer.

CO_2 surface distributions in January and July are shown in Fig. 8 from model simulations with the above emission scenarios and the Conv2 cloud convection transport scheme. Interestingly, with an increasing uptake of NEP, the July surface CO_2 mixing ratios simulated using Conv2 become similar to that in our standard simulation, i.e. simulation using Conv1 and Emi1 (Fig. 3 (top panel)). Compared with Emi1 (Fig. 3 (bottom panel, right-hand column)), July CO_2 mixing ratio is suppressed about 4 and 8 ppm over Asia boreal forest for Emi2 and Emi3,

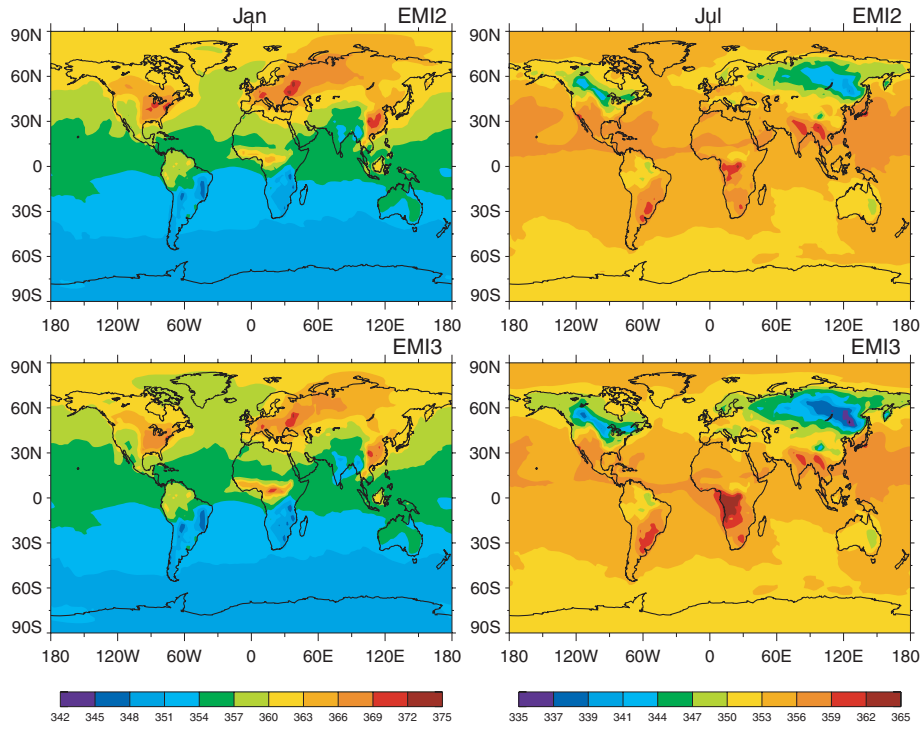

Fig. 8. CO_2 (ppm) surface contours at January (left-hand panel) and July (right-hand panel) using three emissions with Conv2. Note the results corresponding to the EMI1 with Conv2 are shown in Fig. 3 (bottom panel).

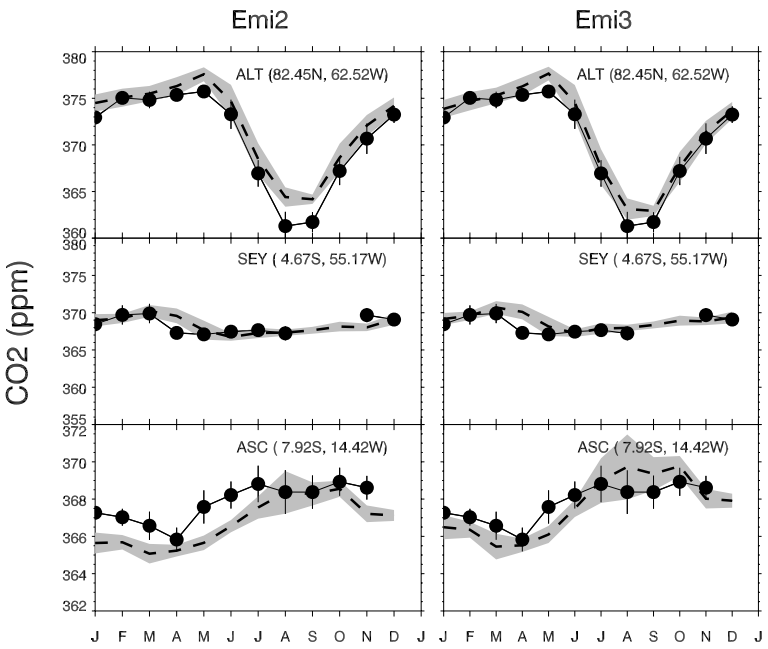

Fig. 9. Same as Fig. 2, but using three emissions with Conv2. Note the result corresponding to EMI1 with Conv2 is shown in Fig. 2 (right-hand column).

respectively (Fig. 8). Furthermore, adjustment of the NH biosphere flux exhibits global implications: global surface CO_2 in July is decreased due to the stronger biosphere uptake except in regions with local fossil fuel and/or biomass burning emissions. In January, the CO_2 surface mixing ratios from the Emi1 and Emi2 emission scenarios are similar except over the SH forest regions (south America, south Africa and Australia) where CO_2 from Emi2 (Fig. 8 (top panel, left-hand column)) is about 0.2 ppm lower than that from Emi1 (Fig. 3 (bottom panel, left-hand column)) due to the increase of CO_2 loss in the SH growing season. Since Emi3 includes biomass burning emission, the CO_2 discrepancy between Emi1 and Emi3 is larger than between Emi1 and Emi2, but the difference is still less than 1 ppm.

Simulated surface CO_2 mixing ratios with three emissions are also compared with CMDL observations in Fig. 9. The discrepancies identified in Section 3.1 with using Emi1 have now become reduced or disappeared with the use of Emi3. Specifically, the improvement has happened at the stations in NH middle and high latitudes, such as ALT. The improvement at these stations in July is attributed to the enhancement of CO_2 uptake in NH boreal forests. The adjustment of biomass burning brings a slightly better agreement in model-observation comparison in station ASC. However, the misrepresentation of tracer concentration during ITCZ at station SEY remains.

4. Conclusions

Quantification of the uncertainty of model behaviour is essential although the acceptable level of uncertainty depends on the application. We present in this paper an evaluation of uncertainties of convective transport parameterization by using two different implementation schemes in a single offline CTM framework, driven by the same meteorological fields. The referred two methods represent cloud convective transport from a simple form to a more complex form. The discrepancies arising from the different approaches are the largest in the NH middle latitudes in summer season, which is attributed primarily to the season's deep cloud activities that are represented differently in the two approaches. It confirms and explains the previous finding from TransCom-3 that the model results vary the most during the growing season (summer) in the northern land regions (Gurney et al., 2004). Furthermore, the largest discrepancy between Conv1 and Conv2 is 7.8 ppm of CO_2, which is about 30% of the CO_2 seasonality for that area. The message conveyed from our study is that, even with the same archived cloud fluxes, different implementation produces substantial discrepancy in the CO_2 distribution. Varying methods of subgrid convective parameterization among different models are likely to produce comparable or even larger differences. This reinforces the crucial importance of quantifying the convective transport error in CO_2 simulations.

Our work also shows that the impact of convection error depends not only on the representation of convection cloud transport in a model, but also on the collocation of deep cloud convection and tracer surface fluxes. Therefore, it is not sufficient to estimate the convection uncertainty for CO_2 simulation through the use of inert tracers with known emissions and atmospheric observations, such as Rn and SF_6. We need to use CO_2 itself.

The emission scenario complied by TransCom 3 and two alternate emission scenarios based on IPCC, 2001 are used to address how these transport uncertainties compare to those in CO_2 source and sink distributions. The investigation indicates that differences between the convective transport forms have

similar magnitude of uncertainty as the emissions, in the context of agreement between CO_2 simulations and observations. This result highlights the complexity of simulating atmospheric CO_2, where balances between different processes (in this case convective transport and emission) can obscure the physical nature of relationships within the system.

The model simulation using the Conv1 approach corresponds better with several aspects of the observations when using TransCom emissions and GEOS-4 winds. On the other hand, the Conv2 approach implements a more complete representation of the convective processes, which should be more physically realistic. Although Conv2 in the standard scenario does not compare as well with observations, the difference is comparable to that produced by known uncertainties in the CO_2 surface fluxes. Thus, we cannot infer that one method is conclusively better than the other. We can infer that the different CO_2 fields produced by the two methods will produce different seasonal source/sink distributions in the context of an inverse calculation, and we can use the magnitude of the difference here as one estimate of model transport uncertainty. We also recognize that different models have quite different methods of parameterizing subgrid mass fluxes and tracer transport, that these differences may contribute significant uncertainty in global CO_2 transport and source/sink inference, and that very likely none of these parameterizations is quantitatively accurate in representing real-world meteorology.

5. Acknowledgements

This work has been supported by the NASA Carbon Cycle Science and NASA Atmospheric Chemistry Modeling and Analysis Program (ACMAP). The observational CO_2 data are provided by the NOAA CMDL Carbon Cycle Cooperative Global Air Sampling Network.

References

Andres, R. J., Marland, G., Fung, I. and Matthews, E. 1996. Distribution of carbon dioxide emissions from fossil fuel consumption and cement manufacture, 1950-1990 *Gobal Biogeochem. Cycles* **10**, 419–429.

Aubinet, M., Chermanne, B., Vandenhaute, M., Longdoz, B., Yernaux, M. and co-authors. 2001. Long term carbon dioxide exchange above a mixed forest in the Belgian Ardennes. *Agric. For. Meteorol.* **108**, 293–315.

Battle, M., Bender, M. L., Tans, P. P., White, J. W. C., Ellis, J. T. and co-authors. 2000. Global carbon sinks and their variability inferred from atmospheric O_2 and d13C. *Science* **287**, 2467–2470.

Bey, I., Jacob, D. J., Yantosca, R. M., Logan, J. A., Field, B. D. and co-authors. 2001. Global modeling of tropospheric chemistry with assimilated meteorology: model description and evaluation. *J. Geophys. Res.* Vol. **106**(D19), 23 073–23 078 (2001JD000807).

Bloom, S., da Silva, A., Dee, D., Bosilovich, M., Chern, J-D and co-authors. 2005. Documentation and Validation of the Goddard Earth Observing System (GEOS) Data Assimilation System-Version 4, NASA/TM-2005-104606, Vol. 26.

Bousquet, P., Peylin, P., Ciais, P., Le Quere, C., Friedlingstein, P. and co-authors. 2000. Regional changes in carbon dioxide fluxes of land and oceans since 1980. *Science* **290**, 1342–1346.

Chin, M., Ginoux, P., Kinne, S., Torres, O., Holben, B. N. and co-authors. 2002. Tropospheric aerosol optical thickness from the GOCART model and comparisons with satellite and sun photometer measurements. *J. Atmos. Sci.* **59**, 461–483.

Chin, M., Chu, A., Levy, R., Remer, L., Kaufman, Y. and co-authors. 2004. Aerosol distribution in the northern hemisphere during ACE-Asia: results from global model, satellite observations, and sunphotometer measurements. *J. Geophys. Res.*, **109**, doi: 10.1029/2004JD004829.

Collins, B., Leo, D., Hack, J., Randall, D., Rasch, P. and co-authors. 2004. Description of the NCAR Community Atmosphere Model (CAM 3.0), http://www.ccsm.ucar.edu/models/atm-cam/docs/description/.

Denning, A. S., Collatz, G. J., Zhang, C., Randall, D. A., Berry, J. A. and co-authors. 1996. Simulations of terrestrial carbon metabolism and atmospheric CO_2 in a general circulation model. Part 1: surface carbon fluxes. *Tellus* **48B**, 521–542.

Denning, A. S., Holzer, M., Gurney, K. R., Heimann, M., Law, R. M. and co-authors. 1999. Three-dimensional transport and concentration of SF6-A model intercomparison study (TransCom 2). *Tellus* Ser. B, **51**, 266–297.

Douglass, A. R., Schoeberl, M. R., Rood, R. B. and Pawson, S. 2003. Evaluation of transport in the lower tropical stratosphere in a global chemistry and transport model *J. Geophys. Res.* **108**(D9), 4259, doi:10.1029/2002JD002696.

Eneroth, K., Kjellström, E. and Holmén, H. 2003a. A trajectory climatology for Svalbard investigating how atmospheric flow patterns influence observed tracers concentrations. *Phys. Chem. Earth* **28**, 1191–1203.

Eneroth, K., Kjellstrom, E. and Holmen K. 2003b. Interannual and seasonal variations in transport to a measuring site in western Siberia and their impact on the observed atmospheric CO_2 mixing ratio. *J. Geophys. Res.* **108**(D21), 4660.

Engelen, R., Denning, A. S., Gurney, K. R. and TransCom3 modelers. 2002. On error estimation in atmospheric CO_2 inversions. *J. Geophys. Res.* **107**(D224635), doi: 10.1029/2002JD002195.

Fan, S., Gloor, M., Mahlman, J., Pacala, S., Sarmiento, J. and co-authors. 1998. A large terrestrial carbon sink in North America implied by atmospheric and oceanic carbon dioxide data and models. *Science* **282**, 442–446.

Gerbig, C., Lin, J. C., Wofsy, S. C., Daube, B. C., Andrews, A. E. and co-authors. 2003. Toward constraining regional-scale fluxes of CO_2 with atmospheric observations over a continent. 1: observed spatial variability from airborne platforms. *J. Geophys. Res.* **108**(D24), 4756.

Gilliland, A. B. and Hartley, D. E. 1998. Interhemispheric transport and the role of convective parameterizations. *J. Geophys. Res.* **103**(D17), 22 039–22 046.

Gurney, K. R., Law, R. M., Denning, A. S., Rayner, P. J., Baker, D. and co-authors. 2002. Towards robust regional estimates of CO_2 sources and sinks using atmospheric transport models. *Nature* **415**, 626–630.

Gurney, K. R., Law, R. M., Denning, A. S., Rayner, P. J., Baker, D. and co-authors. 2003. TransCom 3 CO_2 inversion intercomparison. 1: annual mean control results and sensitivity to transport and prior flux information. *Tellus* **55B**, 555–579.

Gurney, K. R., Law, R. M., Denning, A. S., Rayner, P. J., Pak, B. C. and co-authors. 2004. Transcom 3 inversion intercomparison: model mean

results for the estimation of seasonal carbon sources and sinks. *Global Biogeochem. Cycles* **18**, GB1010, doi: 10.1029/2003GB002111.

Hack, J. J. 1994. Parameterization of moist convection in the National Center for Atmospheric Research community climate model (CCM2). *J. Geophys. Res.* **99**, 5551–5568.

Intergovernmental Panel on Climate Change (IPCC). 2001. Climate Change 2001: Synthesis Report: Third Assessment Report of the Intergovernmental Panel on Climate Change, Cambridge University Press, New York.

Kawa, S. R., Erickson III, D. J., Pawson, S. and Zhu, Z. 2004. Global CO_2 transport simulations using meteorological data from the NASA data assimilation system. *J. Geophys. Res.* **109**(D18312), doi: 10.1029/2004JD004554.

Law, R. M., Rayner, P. J., Denning, A. S., Erickson, D., Fung, I. Y. and co-authors. 1996. Variations in modeled atmospheric transport of carbon dioxide and the consequences for CO_2 inversions. *Global Biogeochem. Cycles* **10**, 783–796.

Li, Q. B., Jiang, J. H., Wu, D. L., Read, W. G., Livesey, N. J. and co-authors. 2005. Convective outflow of South Asian pollution: a global CTM simulation compared with EOS MLS observations. *Geophys. Res. Lett.* **32**(L14826).

Lin, S. and Rood, R. B. 1996. Multidimensional flux-form semi-Lagrangian transport schemes. *Mon. Weather Rev.* **124**, 2046–2070.

Mahowald, N. M., Rasch, P. J. and Prinn, R. G. 1995. Cumulus parameterizations in chemical transport models. *J. Geophys. Res.* **100**(D12), 26 173–26 189.

Maksyutov, S., Machida, T., Mukai, H., Patra, P. K., Nakazawa, T. and TransCom 3 modelers. 2003. Effect of recent observations on Asian CO_2 flux estimates by transport model inversions. *Tellus* **55B**, 522–529.

Millet, D. B., Jacob, D. J., Turquety, S., Hudman, R. C., Wu, S. and co-authors. 2006. Formaldehyde distribution over North America: implications for satellite retrievals of formaldehyde columns and isoprene emission. *J. Geophys. Res.*, in press.

Murayama, S., Taguchi, S. and Higuchi, K. 2004. Internannual variation in the atmospheric CO_2 growth rate: role of atmospheric transport in the Northern Hemisphere. *J. Geophys. Res.* **109**(D02305), doi:10.1029/2003JD003729.

Olivie, D. J. L., van Velthoven, P. F. J., Beljaars, A. C. M. and Kelder, H. M. 2004. Comparison between archived and off-line diagnosed convection mass fluxes in the chemistry transport model TM3. *J. Geophys. Res.* **109**(D11303), doi:10.1029/2003JD004036.

Olsen, S. C. and Randerson, J. T. 2004. Differences between surface and column atmospheric CO_2 and implications for carbon cycle research. *J. Geophy. Res.* **109**(D02301), doi:10.1029/2003JD003968.

Palmer, P. I., Jacob, D. J., Jones, D. B. A., Heald, C. L., Yantosca, R. M. and co-authors. 2003. Inverting for emissions of carbon monoxide from Asia using aircraft observations over the western Pacific. *J. Geophys. Res.* **108**(D21), 8828, doi:10.1029/2003JD003397.

Randerson, J. T., Thompson, M. V., Conway, T. J., Fung, I. Y. and Field, C. B. 1997. The contribution of terrestrial sources and sinks to trends in the seasonal cycle of atmospheric carbon dioxide. *Global Biogeochem. Cycles* **11**, 535–560.

Randerson, J. T., van der Werf, G. R., Collatz, G. J., Giglio, L., Still, C. J. and co-authors. 2005. Fire emissions from C3 and C4 vegetation and their influence on interannual variability of atmospheric CO_2 and d13CO_2. *Global Biogeochem. Cycles* **19** (Art. no. GB2019).

Rannik, U., Aubinet, A., Kurbanmuradov, O., Sabelfeld, K. K., Markkanen, T. and co-authors. 2000. Footprint analysis for measurements over a heterogeneous forest. *Boundary Layer Meteorol.* **97**, 137–166.

Suntharalingam, P., Randerson, J. T., Krakauer, N., Jacob, D. J. and Logan, J. A. 2005. The influence of reduced carbon emissions and oxidation on the distribution of atmospheric CO_2: implications for inversion analyses. *Global Biogeochem. cycles* **19**(GB4003), doi:10,1029/2005GB002466.

Takahashi, T., Sutherland, S. C., Sweeney, C., Poisson, A., Metzl, N. and co-authors. 2002. Global sea-air CO_2 flux based on climatological surface ocean pCO_2, and seasonal biological and temperature effects, *Deep-Sea Res. II* **49**, 1601–1622.

Tans, P. P., Fung, I. Y. and Takahashi, T. 1990. Observational constraints on the global atmospheric CO_2 budget. *Science* **247**, 1431–1438.

Van der Werf, G. R., Randerson, J. T., Collatz, G. J. and Giglio, L. 2003. Carbon emissions from fires in tropical and subtropical ecosystems. *Global Change Biol.* **9**, 547–562.

Van der Werf, G. R., Randerson, J. T., Collatz, G. J., Giglio, L., Kasibhatla, P. S. and co-authors. Continental-scale partitioning of fire emissions during the 1997–2001 El Nino/La Nino period. *Science* **303**, 73–76.

Yi, C., Davis, K. J., Bakwin, P. S., Denning, A. S., Zhang, N. and co-authors. 2004. Observed covariance between ecosystem carbon exchange and atmospheric boundary layer dynamics at a site in northern Wisconsin. *J. Geophys. Res.* **109**(D08302), doi:10.1029/2003JD004164.

Zender, C. S., Bian, H. and Newman, D. 2003. The mineral dust entrainment and deposition (DEAD) model: description and global dust distribution *J. Geophys. Res.* **108**, 4416.

Zhang, G. J. and McFarlane, N. A. 1995. Sensitivity of climate simulations to the parameterization of cumulus convection in the Canadian climate center general-circulation model. *Atmos. Ocean* **33**, 407–446.